Strain and stacking registry effects on the hyperbolicity of exciton polaritons in few-layer black phosphorus

Diana M. N. Thomen [1,*] Cem Sevik,[2,3] Milorad V. Milošević,[2,4,†] Lara K. Teles,[1,‡] and Andrey Chaves [5,2,§]

[1]*Grupo de Materiais Semicondutores e Nanotecnologia, Instituto Tecnológico de Aeronáutica, DCTA, 12228-900 São José dos Campos, Brazil*

[2]*Department of Physics & NANOlab Center of Excellence, University of Antwerp, Groenenborgerlaan 171, B-2020 Antwerp, Belgium*

[3]*Department of Mechanical Engineering, Faculty of Engineering, Eskisehir Technical University, 26555 Eskisehir, Turkey*

[4]*Instituto de Física, Universidade Federal de Mato Grosso, Cuiabá, Mato Grosso 78060-900, Brazil*

[5]*Universidade Federal do Ceará, Departamento de Física, Caixa Postal 6030, 60455-760 Fortaleza, Ceará, Brazil*

(Received 6 February 2024; revised 17 May 2024; accepted 22 May 2024; published 10 June 2024)

We analyze, from first-principles calculations, the excitonic properties of monolayer black phosphorus (BP) under strain, as well as of bilayer BP with different stacking registries, as a base platform for the observation and use of hyperbolic polaritons. In the unstrained case, our results confirm the in-plane hyperbolic behavior of polaritons coupled to the ground-state excitons in both mono- and bilayer systems, as observed in recent experiments. With strain, we reveal that the exciton-polariton hyperbolicity in monolayer BP is enhanced (reduced) by compressive (tensile) strain in the zig-zag direction of the crystal. In the bilayer case, different stacking registries are shown to exhibit hyperbolic exciton polaritons with different dispersion, while also peaking at different frequencies. This renders both mechanical stress and stacking registry control as practical tools for tuning physical properties of hyperbolic exciton polaritons in black phosphorus, which facilitates detection and further optoelectronic use of these quasiparticles.

DOI: 10.1103/PhysRevB.109.245413

I. INTRODUCTION

Few-layer black phosphorus (BP) [1] stands out amongst the two-dimensional (2D) semiconductors due to its direct gap at the Γ point of the Brillouin zone for any number of layers, along with a strong anisotropy of the band curvatures around this point, which yields linear dichroism [2] and anisotropic effective masses for both conduction- and valence-band states. It has been demonstrated both theoretically [3] and experimentally [4] that, due to the strong anisotropy of the BP crystal lattice, the selection rules for light absorption/emission involving ground-state excitons in this material (at ≈1.5–1.9 eV) requires linearly polarized light along the armchair direction of the BP crystal, while polarization along the zig-zag direction produces practically no effect at energies below 2.5 eV.

Absorption peaks are associated with peaks in the imaginary part of the dielectric function ε. Provided the peak is sufficiently narrow and intense, the real part of the dielectric function may reach negative values in the vicinity of the peak frequency. Intense exciton peaks are expected in 2D materials such as BP, due to the weak dielectric screening of electron-hole interactions in the surroundings of the material layer, which yields strong exciton binding energies [5]. Moreover, narrow peaks have been experimentally obtained in several 2D materials, via control of the material quality and/or encapsulation with other materials [6]. Therefore, excitonic peaks in few-layer BP are indeed expected to lead to negative $\mathrm{Re}[\varepsilon]$ in the vicinity of the ground-state exciton frequency, but only for the armchair direction ($\mathrm{Re}[\varepsilon_{xx}] < 0$), whereas the absence of a peak in ε_{yy} at this frequency, resulting from the linear dichroism of BP induced by its crystal anisotropy, yields $\mathrm{Re}[\varepsilon_{yy}] > 0$.

A spherically symmetric dispersion for the polariton involved in the light absorption is expected if the dielectric function at the polariton frequency is the same in all directions. However, a dielectric function that is different in one or more directions at the polariton frequency leads to elliptical dispersion if all values of the dielectric function have the same sign. A yet more exotic case occurs when the sign of the dielectric function at this frequency is different for one of the directions: in this case, the polariton dispersion becomes hyperbolic [7]. Consequently, the expected $\mathrm{Re}[\varepsilon_{yy}]\mathrm{Re}[\varepsilon_{xx}] < 0$ in the vicinity of excitonic peaks of few-layer BP, as previously mentioned, may result in a light dispersion that is hyperbolic *in the plane* for polaritons [8,9] in this material.

Although such in-plane hyperbolicity has been already observed for phonon and plasmon polaritons [10–18], it has not been extensively investigated yet with exciton polaritons. Actually, most layered 2D semiconductors exhibit strong anisotropy between in-plane and out-of-plane coordinates, which already suggests the possibility of observing exciton polaritons with hyperbolic dispersion along the out-of-plane direction. Even so, only very recently the experiments were able to probe out-of-plane exciton-polariton hyperbolicity in few-layer WSe_2 [19] and layered perovskites [20].

*Contact author: diana.thomen@ga.ita.br
†Contact author: milorad.milosevic@uantwerpen.be
‡Contact author: lkteles@ita.br
§Contact author: andrey@fisica.ufc.br

Due to the previously mentioned strong in-plane anisotropy of its band structure and polarizabilities, BP emerges as a particularly suitable platform for further investigation of in-plane hyperbolic exciton polaritons. Indeed, $\mathrm{Re}[\varepsilon_{yy}]\mathrm{Re}[\varepsilon_{xx}] < 0$ around the ground-state exciton features of few-layer BP has been recently experimentally probed, where it was demonstrated that the range of frequencies where hyperbolic exciton-polariton dispersion is observed decreases with increasing the number of BP layers [21]. Alternative strategies to increase the range of frequencies where hyperbolicity can be observed would be helpful for a deeper investigation of this interesting, yet elusive, phenomenon.

In this study, we explore techniques to modulate excitonic effects in 2D in-plane anisotropic semiconductors, focusing specifically on the in-plane hyperbolicity of excitons in 2D BP structures. We have used *ab initio* methods within the density functional theory (DFT) and G_0W_0 corrections to perform electronic structure calculations. Bethe-Salpeter equations (BSE) are employed to determine the dielectric function in the presence of excitons. Our results for narrow excitonic peaks in unstrained monolayer and bilayer BP show a theoretical confirmation of the in-plane hyperbolic behavior of the ground-state exciton observed in recent experiments [21], where similarly narrow excitonic features are measured in this few-layer material. Furthermore, our calculations for monolayer BP under compressive (tensile) strain show significant enhancement (reduction) of the excitonic features observed around 1.5 eV for light polarized in the armchair direction, which eventually leads to an enhanced (reduced) dip in the real part of the dielectric function in the vicinity of the exciton energy and, consequently, an enhanced (reduced) hyperbolicity of the polariton modes associated with these excitonic states. In addition to strain modulation, we explored the potential of altering BP stacking configurations. We observe that the energy of the $\mathrm{Re}[\varepsilon_{xx}]$ peaks undergoes shifts when the stacking type is varied, suggesting a feasible strategy to control the frequency of this phenomenon via stacking modifications. Additionally, we examined the effect of applying strain in the out-of-plane direction of the BP bilayer, where results indicated that strains up to ≈4% produce shifts in the energy range while keeping the hyperbolic character of the exciton polaritons robust.

The paper is organized as follows. Section II describes the theoretical model and computational details used in the calculations of excitonic properties and polariton isofrequency lines of monolayer and bilayer BP. In Sec. III, the main results are shown and relevant discussions are made on the control of exciton polaritons via strain and stacking registry engineering. Finally, we present our conclusions in Sec. IV.

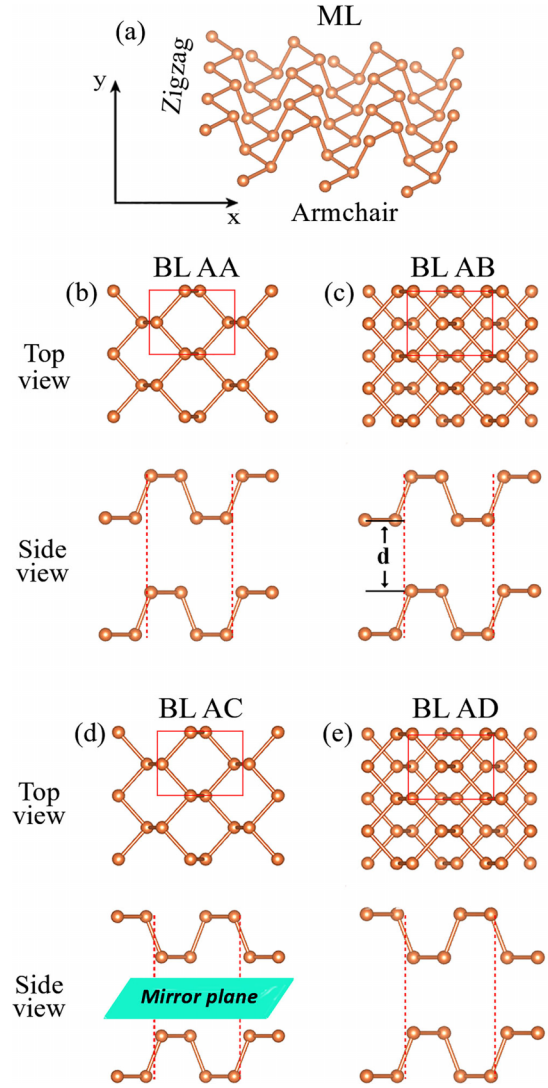

FIG. 1. Supercells utilized for simulating BP monolayer (ML) and bilayer (BL) structures. (a) Perspective view of the ML, highlighting both zig-zag and armchair directions. Top and side views of BL for different stackings: (b) AA, (c) AB, (d) AC, and (e) AD. The interlayer distance, denoted by d, is also shown.

II. COMPUTATIONAL DETAILS

Many-body perturbation theory calculations were performed as implemented in the YAMBO code [22] for the monolayer (ML) structure illustrated in Fig. 1(a). Four atoms were used in the composition of the ML unit cell. The G_0W_0 [23,24] corrections to the Kohn-Sham eigenvalues were calculated with the plasmon-pole approximation for the dynamical electronic screening. The electronic energies including band gap were converged with a $46 \times 34 \times 1$ k-grid mesh, 432 k points in the irreducible Brillouin zone (BZ), summing over 330 states for both the screening and the Green's functions. The G_0W_0 corrections were obtained for the top three valence bands and the bottom four conduction bands. The BSE calculations were performed with random-phase approximation static screening, which was summed over 300 bands and in the Tamm-Dancoff approximation on top of the GW results. The exciton energies and their wave functions were calculated for the first 10 000 excitonic states by using the iterative scheme enabled by the SLEPC library [25]. The Coulomb cutoff of 40 Å was used along the out-of-plane direction to eliminate the interactions to all the undesired images of the systems in both G_0W_0 and BSE steps [26]. The GW + BSE method employed here

is standard in the calculation of excitonic properties of undoped BP, (see, e.g., Refs. [27,28]), whereas the use of other approaches, such as those beyond plasmon-pole approximation [29], which would improve accuracy (although being more computationally challenging), or those involving GW + cumulant methods [30], which may be used for investigating other complex quasiparticles, such as plasmarons [31], is left for discussion in future works.

The desired wave functions and corresponding energies for the YAMBO calculations are obtained from density functional theory as implemented in QUANTUM ESPRESSO code [32] using Perdew-Burke-Ernzerhof [33] correlation including norm-conserving fully relativistic generalized gradient approximation type pseudopotentials [34] generated by the PSEUDODOJO project [35]. Here, the plane-wave energy cutoff, the vacuum distance between two periodic layers, and the k-grid sampling are taken as 100 Ry, 42 a.u., and $46 \times 34 \times 1$, respectively. We adopted Grimme's dispersion correction (labeled as Grimme-D2 in QUANTUM ESPRESSO) [36,37] for accurate description of van der Waals interactions in the considered systems.

The dielectric components in the 2D level are obtained using the following formula [38,39],

$$\epsilon = 1 + \frac{4\pi\alpha_{2D}}{d}, \tag{1}$$

where α_{2D} is the polarizability per surface unit obtained via the YAMBO code [40], and d is the thickness of a monolayer black phosphorus, 10.60 a.u., approximated as the average interlayer distance in bulk BP.

Bilayer calculations for the stacking registries illustrated in Figs. 1(b)–1(e) were performed by using the Vienna Ab initio Simulation Package (VASP) [41]. The unit cells of the BLs were assembled using eight atoms. Optical properties were obtained with the G_0W_0 method, and the addition of excitonic effects was performed using the Bethe-Salpeter equation [42]. The k-point grid adopted was $18 \times 18 \times 1$ and the cutoff energy for the plane-wave base was 380 eV. The vacuum distances in each structure were adopted according to previous refinement tests and were around 20 Å. Throughout the paper, the parameter referring to the complex shift δ in the Kramers-Kronig transformation was considered to be on the order of $\approx$0.01 eV, and consequently, the number of grid points on which the density of states was evaluated was adjusted to 4000.

Polaritons confined in a 2D slab of width d surrounded by vacuum obey a dispersion relation obtained from Maxwell equations as [43]

$$\bar{\sigma}_{xx}\left(k_x^2 - k_0^2\right) + \bar{\sigma}_{yy}\left(k_y^2 - k_0^2\right) = ik_0k(1 + 4\pi^2\bar{\sigma}_{xx}\bar{\sigma}_{yy}), \tag{2}$$

where $k_0 = \omega/c$ is the light wave number at a given energy $E = \hbar\omega$ and the optical conductance, obtained from the dielectric function in Eq. (1), is in the dimensionless form $\bar{\sigma}_{ii} = \sigma_{ii}d/c$. Since Eq. (2) involves nonlinear terms in k_x and k_y, as well as real and imaginary components, solving this equation as it is is a challenging task. Therefore, we take reasonable approximations to simplify this equation and solve it in a more convenient way: assuming that the light wave vector is much smaller than the polariton wave vector $\vec{k} = k_x\hat{x} + k_y\hat{y}$ and that the real part of σ_{ii} (proportional to the light absorption rate) is small at a given ω, this equation reduces approximately to

$$\frac{k_x^2}{\bar{\sigma}_{xx}} + \frac{k_y^2}{\bar{\sigma}_{yy}} - 2\pi k_0 k\left(\frac{1}{4\pi^2\bar{\sigma}_{xx}\bar{\sigma}_{yy}} - 1\right) = 0. \tag{3}$$

These conditions are indeed met in the vicinity of an exciton peak. In the following section, isoenergy curves for exciton polaritons in reciprocal space, calculated with Eq. (3), are provided, so as to emphasize the elliptical/hyperbolic nature of these quasiparticles.

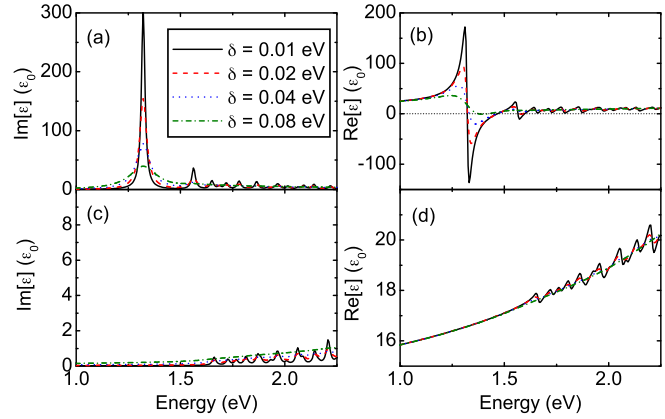

FIG. 2. Imaginary (left panels) and real (right panels) parts of the dielectric function for monolayer BP in the armchair (a, b) and zig-zag (c, d) directions. Four values for the peak broadening δ are considered. The horizontal dotted line in panel (b) at $\mathrm{Re}[\varepsilon] = 0$ is a guide for the eye.

III. RESULTS AND DISCUSSION

A. Monolayer BP and strain effects

High-quality monolayer BP samples exhibit pronounced ground-state exciton ($1s$) peaks with a typical energy broadening of a few tens of meV [44–47]. DFT calculations of such excitonic peaks with different values for the energy broadening δ are shown in Fig. 2. Absorption coefficients for linearly polarized light in the armchair and zig-zag directions are proportional to $\mathrm{Im}[\varepsilon_{xx}]$ and $\mathrm{Im}[\varepsilon_{yy}]$, which are shown in Figs. 2(a) and 2(c), respectively. The ground-state exciton peak at $\approx$1.3 eV is observed only in $\mathrm{Im}[\varepsilon_{xx}]$, as a result of the strong anisotropy of BP, which leads to its experimentally observed linear dichroism [2]. Consequently, $\mathrm{Re}[\varepsilon_{xx}]$ is strikingly different from $\mathrm{Re}[\varepsilon_{yy}]$, as shown in Figs. 2(b) and 2(d), respectively. Specifically, $\mathrm{Re}[\varepsilon_{yy}]$ is positive over the whole range of energies shown in Fig. 2(d), whereas $\mathrm{Re}[\varepsilon_{xx}]$ is negative, e.g., within a 0.145-eV range of energies in the vicinity of the $1s$ peak for $\delta = 0.020$ eV in Fig. 2(b).

Notice that, so far, the $2s$ exciton peak of few-layer BP has not been detected in experiments with the same narrow energy width as the one observed for $1s$. However, since all exciton peaks in our model are calculated with the same broadening δ, as an approximation, our results also show another narrow energy range at slightly higher energy where $\varepsilon_{xx} < 0$, resulting from the $2s$ exciton peak. In fact, although not as narrow as the $1s$ peak, the experimentally observed $2s$ exciton peaks

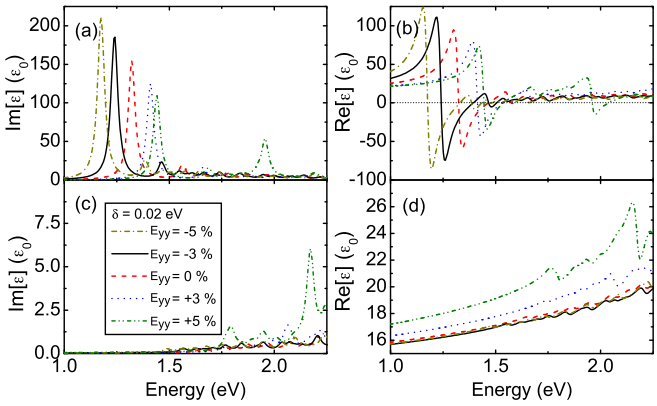

FIG. 3. Imaginary (left panels) and real (right panels) parts of the dielectric function for monolayer BP in the armchair (a, b) and zig-zag (c, d) directions. Four values of uniaxial strain in the zig-zag direction E_{yy} are considered. The horizontal dotted line in panel (b) at $\mathrm{Re}[\varepsilon] = 0$ is a guide for the eye.

in monolayer BP are still strong enough to produce negative $\mathrm{Re}[\varepsilon_{xx}]$ and, consequently, hyperbolic excitons, in agreement with our results [21].

From the results in Fig. 2, it is clear that the narrower the broadening δ of the excitonic peak is the wider is the energy range where $\mathrm{Re}[\varepsilon_{xx}]\mathrm{Re}[\varepsilon_{yy}] < 0$, i.e., where a hyperbolic exciton polariton is expected. From here onward, we keep $0.01 \leqslant \delta \leqslant 0.02$ eV, which is close to the experimentally observed energy broadening in Ref. [46].

Figure 3 shows that, as compressive (negative) strain is applied in the zig-zag direction, the exciton features in $\mathrm{Re}[\varepsilon_{xx}]$ are all enhanced, which increases the energy range of hyperbolicity for exciton polaritons. On the other hand, tensile (positive) strain strongly decreases the exciton peak intensity and, consequently, the hyperbolicity range. This is more clearly observed in Fig. 4, which shows the edges of the hyperbolicity regions for 1*s* and 2*s* excitons in monolayer BP as a function of strain in the zig-zag direction. We have also calculated the hyperbolicity ranges as a function of strain in the armchair direction, which are shown as dashed lines in Fig. 4. Tensile strain in the armchair direction reduces the hyperbolicity range to the point that, for 2*s* excitons, it is not visible for any positive strain in Fig. 4. It is also clear from Fig. 4(b) that only strain in the armchair direction tunes the width of the hyperbolic exciton-polariton spectrum, whereas strain in the zig-zag direction changes only the position of the excitonic peaks while keeping the hyperbolicity range almost the same. From these results, it becomes clear that hyperbolic excitons are easier to observe either in pristine monolayer BP or in a sample with tensile strain in the armchair direction.

Consequences of such strain dependence of ε in monolayer BP are also expected to be significant in wrinkled monolayer samples, such as the one sketched in Fig. 5(a). Monolayer BP may become rippled and undergo modulated strain when placed on top of an elastomeric substrate (see, e.g., Ref. [48]). The period of these ripples is ≈500 nm in length, thus creating wide regions where the system is locally under tensile strain, relaxed, or under compressive strain, as illustrated by the regions labeled as (I), (II), and (III) in

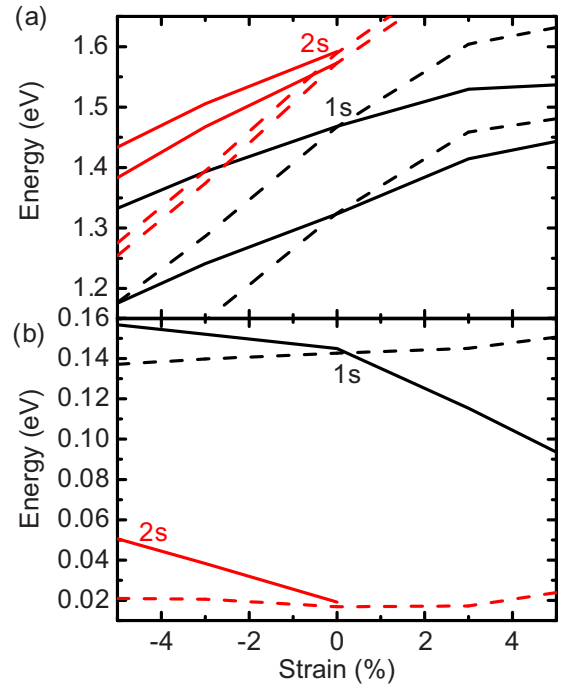

FIG. 4. (a) Energy boundaries where hyperbolic exciton polaritons are expected in the ground (1*s*, black) and first excited (2*s*, red) exciton states of monolayer BP as a function of strain in the zig-zag (dashed) and armchair (solid) directions. $\mathrm{Re}[\varepsilon_{xx}]\mathrm{Re}[\varepsilon_{yy}] < 0$ is observed in between the lines of the same type in the energy spectrum. (b) Range of energies where hyperbolic exciton polaritons are expected for the states shown in panel (a).

Fig. 5(a), respectively. The exciton-polariton dispersions for −5% (yellow dashed-dotted curve), 0 (red dashed curve), and +5% (green dashed-dotted-dotted curve) strained monolayer BP at the exciton peak frequency of each of these cases, shown in Fig. 5(b), exhibit different propagation directions, since the propagation direction is perpendicular to the isoenergy curves. Figure 3 shows that compressive strain in monolayer BP leads to the reduced exciton energy; therefore, one expects ground-state excitons to be formed in these regions of the rippled layer. Thus, assuming a wrinkled monolayer BP with a strain distribution ranging from −3% to +3%, as one fixes the exciton-polariton frequency to that corresponding to the energy of the exciton the compressed region leads to a polariton dispersion that is modulated along the ripple, being hyperbolic in the compressive strain region, while being elliptical in the relaxed and tensile strain regions. The consequences of such a space-dependent polariton dispersion for light propagation along the rippled monolayer BP require properly solving Maxwell equations for such a system, which is beyond the scope of this paper and is therefore left as an exciting topic for future works.

B. BP bilayers: stacking order and pressure effects

Bilayers provide a unique environment to enable extra tunability of excitonic properties, especially due to interlayer coupling interactions. Therefore, it is important to investigate

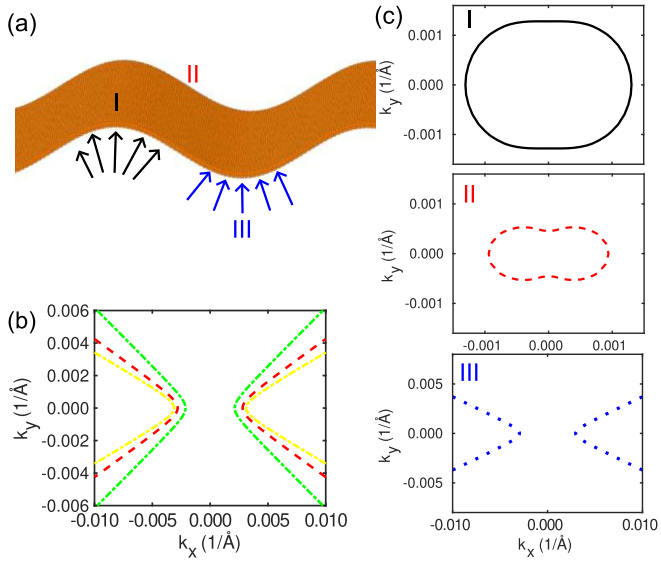

FIG. 5. (a) Sketch of a wrinkled monolayer BP, where a uniaxial distribution of strain is observed, as represented by different regions: (I) tensile strain, (II) unstrained, and (III) compressive strain [48]. (b) Isoenergy curves in the exciton-polariton dispersion for different values of strain. Curves are calculated at the energy of most negative Re[ε_{xx}] in Fig. 3(b) for each value of strain. (c) The bottom panel shows the isoenergy curve of the exciton-polariton dispersion at the $E_{xx} = -3\%$ region in the wrinkled monolayer BP illustrated in panel (a). As observed in Fig. 3(a), this exciton has lower energy as compared to the other regions with different strain values in the sample. Results at the $E_{xx} = 0\%$ (middle panel) and $E_{xx} = +3\%$ (top panel) strain regions are also shown at the same energy, for comparison.

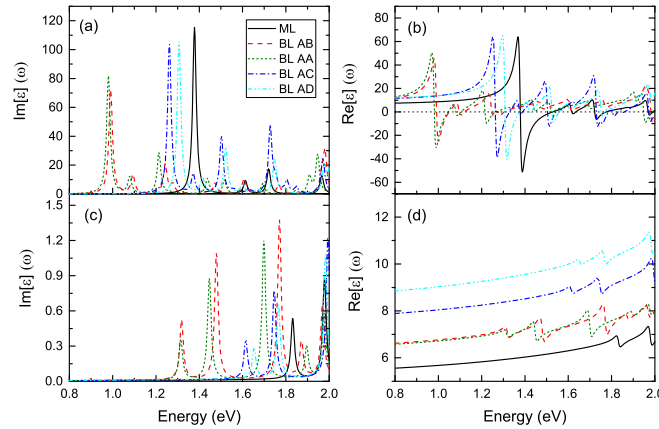

FIG. 6. Imaginary (left panels) and real (right panels) parts of the dielectric function for BP monolayer (ML) and bilayers (BL), in the armchair (a, b) and zig-zag (c, d) directions. Four types of bilayers are considered: AB, AA, AC, and AD (see text for description). A $\delta = 0.010$ eV broadening is assumed, and the horizontal dotted line in panel (b) at Re[ε] = 0 is a guide for the eye.

whether these interactions can further modulate the properties of the exciton polaritons studied here. In order to do so, we also explore how different stacking registries and interlayer distances (tunable, e.g., via vertical pressure) might influence the existence and physical properties of hyperbolic exciton polaritons.

We consider BP bilayers (BL) under four distinct stacking orders, as illustrated in Fig. 1: AA (b), AB (c), AC (d), and AD (e), as illustrated in Fig. 1. Figure 6 shows the results of GW + BSE calculations for the different types of BP bilayer stacking, where Figs. 6(a) and 6(c) refer to the imaginary parts of the dielectric function for the armchair and zig-zag directions, respectively, whereas Figs. 6(b) and 6(d) present the real parts of the dielectric function for these same directions. Results for a BP monolayer are shown here for the sake of comparison.

Firstly, notice that all four cases of BL stacking order exhibit optical anisotropy along with a hyperbolic region within some range of energies. In comparison to the monolayer case, we observe that the intensity of the peaks of ε_2 is reduced in bilayers, which also influences ε_1. Nevertheless, the peaks are still intense enough to lead to hyperbolic exciton polaritons, as has been indeed experimentally observed [21]. When comparing the five cases, it becomes clear that the type of stacking considerably affects the values and peak positions of ε_2 in both the armchair direction and the zig-zag direction.

Table I presents the values for the energy boundaries, ω_1 and ω_2, as well as the range of energies, ΔE_{ε_1}, where the lowest-energy hyperbolic exciton polaritons are expected to occur. While the monolayer offers a broader interval for potential hyperbolic exciton polariton occurrence, the bilayer structures, within their specific stacking registries, introduce nuanced variations in energy boundaries. Comparing the bilayer stackings, the AA and AB configurations display very similar energy boundaries, from ≈0.98 to ≈1.06 eV. In contrast, the AC and AD stackings shift toward higher-energy values, with boundaries lying in the range of 1.26 to 1.36 eV. This result emphasizes the significance of the specific stacking order in modulating the polaritonic properties of bilayer BP.

We now focus on the most stable bilayer stacking configuration, namely, AB, and analyze the effect of vertical pressure on the hyperbolic nature of its excitonic peaks. Figure 7 depicts the results for the optical response derived from GW + BSE calculations, when uniaxial pressure is applied along the direction normal to the plane of the BP bilayer AB. As a result of this pressure, represented here as a perpendicular strain E_{zz}, the interlayer distance (d in Fig. 1) decreases. In the absence of such strain, this structure

TABLE I. Energy boundaries (ω_1 and ω_2) and the energy range for which the real part of the dielectric function has a negative value in the armchair direction, while being positive in the zig-zag direction (ΔE_{ε_1}), for the monolayer (ML) case as well as for the four cases of stacking registry (AA, AB, AC, and AD) of the bilayer (BL) case. All values are given in eV.

Structure	ω_1	ω_2	ΔE_{ε_1}
ML	1.38	1.52	0.15
BL AA	0.98	1.05	0.06
BL AB	0.99	1.06	0.06
BL AC	1.26	1.33	0.07
BL AD	1.30	1.36	0.06

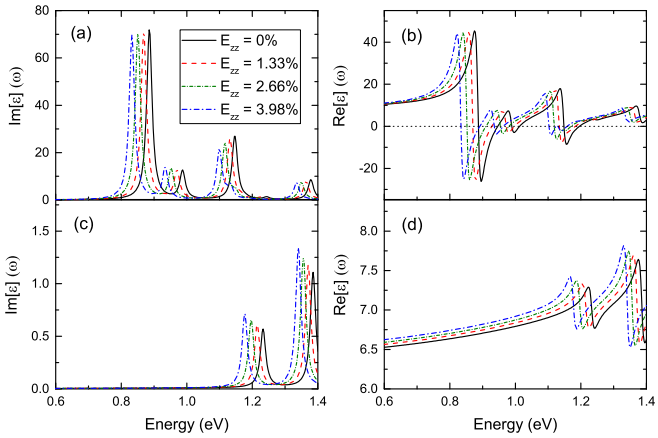

FIG. 7. Imaginary (left panels) and real (right panels) parts of the dielectric function for the AB-type bilayer BP, in the armchair (a, b) and zig-zag (c, d) directions. Three values for strain E_{zz} perpendicular to the BP plane are considered. The horizontal dotted line in panel (b) at $\mathrm{Re}[\varepsilon] = 0$ is a guide for the eye.

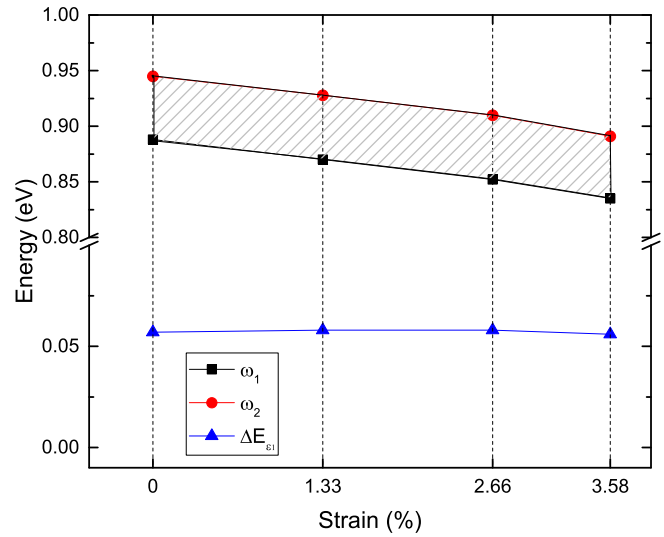

FIG. 8. Range of energies (shaded area) where exciton polaritons with hyperbolic dispersion are expected, as a function of applied strain in the direction perpendicular to the BP plane, considering bilayer BP with AB stacking. The hyperbolicity region lies between ω_1 and ω_2, with width $\Delta E_1 = \omega_2 - \omega_1$.

exhibits a direct gap. However, as documented in previous literature [49], it changes to a metallic state when such strain exceeds 8%. Therefore, our analysis focuses on strain values below 4%, where the bilayer BP retains its semiconducting properties.

Figures 7(a) and 7(c) show the imaginary parts of the dielectric function ε for the armchair and zig-zag directions, respectively, while Figs. 7(b) and 7(d) present the corresponding real parts of ε for the same directions. A strain-induced shift of the $\mathrm{Im}[\varepsilon]$ peaks towards lower-energy levels is observed, as a result of reduced quasiparticle band gaps [49], which leads to a redshift of the energy range where hyperbolic exciton polaritons are expected. However, regarding the energy range where negative values for ε_1 are evident, the application of strain yielded negligible alterations, resulting in a constant range ΔE_{ε_1} of 0.06 eV. This is summarized in Fig. 8, which shows a constant ΔE_{ε_1} (blue triangles) throughout the whole set of strain values considered here, while a hard redshift of the hyperbolic exciton-polariton range (black squares and red circles) is observed.

With the dielectric functions shown in Fig. 6, we evaluate the elliptical/hyperbolic nature of the excitons polaritons in each type of BL stacking, using Eq. (3). For this, we fix the polariton frequency to that corresponding to the energy of the lowest value of the real part of the dielectric function for BL AB [red curve in Fig. 6(b)], namely, 1.0 eV. The isoenergy curves for each type of BL are shown in Fig. 9. In this figure, one observes that polaritons at the same frequency/energy in the various types of stacking will have different characters: in the AA and AB stacking registries, the exciton polaritons exhibit a hyperbolic nature, while in AC and AD, they have an elliptical nature. This behavior is relevant, e.g., when we analyze moiré patterns in twisted BP bilayers: Fig. 9(e) illustrates a moiré pattern in bilayer BP with an interlayer twist $\theta = 5^\circ$, where one observes that, along the extension of the crystal structure, there are regions where the stacking registries are locally different, which results in a space-dependent nature of the exciton-polariton dispersion. Moreover, AA and AB stacking registries are shown to exhibit the lowest exciton energies (see Fig. 6), which implies that the most energetically favorable exciton-polariton state in such a moiré pattern is confined to the vertical quasi-one-dimensional (1D) channel of AA and AB stacking registries illustrated in Fig. 9(e) [50], in which it propagates according to a hyperbolic dispersion, surrounded by elliptic (at 1 eV) exciton-polariton states in the channel formed by AD and AC stacking registries.

IV. CONCLUSIONS

In summary, we have calculated the effective dielectric function of monolayer and bilayer BP in the presence of excitons via DFT with GW corrections, along with the BSE. We predict that a pristine unstrained BP monolayer with a narrow ($\delta = 0.02$ eV, a typical value in experiments involving high-quality samples) exciton peak exhibits in-plane hyperbolic character (i.e., $\mathrm{Re}[\varepsilon_{yy}]\mathrm{Re}[\varepsilon_{xx}] < 0$) within an ≈0.15-eV energy range in the vicinity of the ground-state exciton. Bilayer BP also exhibits in-plane hyperbolic polaritons in the vicinity of the exciton ground state, but with a somewhat lower-energy range, ≈0.06 eV or ≈0.07 eV, depending on the stacking registry. Both results are in good agreement with the recently experimentally observed results for this material [20].

Our results for monolayer BP also demonstrate that, although strain in the zig-zag direction does not significantly change the hyperbolicity range, this range can be tuned via uniaxial strain along the armchair direction: a −5% (+5%) strain in the armchair direction increases (reduces) the energy range in the ground-state peak from 0.145 eV, in the absence of strain, to ≈0.16 eV (≈0.09) eV. This result is also relevant in the context of the experimentally observed wrinkled monolayer BP samples [48], where the strong strain modulation along the BP plane induces a space-dependent dispersion for the exciton polaritons. A similar space-dependent

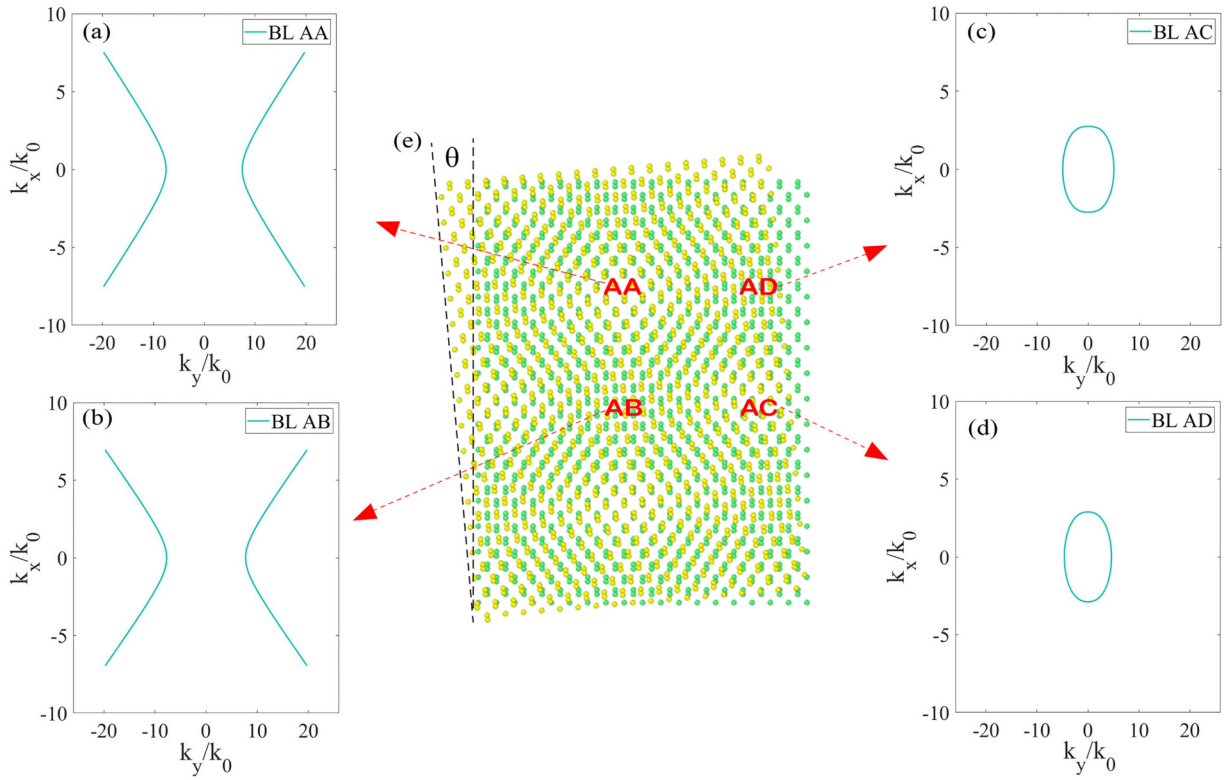

FIG. 9. Isoenergy curves for excitons polaritons in BP bilayers, considering stacking registries (a) AA, (b) AB, (c) AC, and (d) AD, for the polariton energy $E = 1.0$ eV. (e) Sketch of a BP bilayer with interlayer twist angle $\theta = 5°$, forming a moiré pattern with the four types of stacking registries labeled.

dispersion is also expected in twisted bilayer BP: our results demonstrate that the hyperbolic/elliptical nature of the exciton-polariton dispersion strongly depends on the stacking registry. The moiré pattern in twisted bilayer BP, formed by regions where the crystal is locally in the AA, AB, AC, or AD stacking registry, is expected to confine the ground-state exciton in a quasi-1D channel of AA and AB regions, where the polariton dispersion is locally hyperbolic, whereas the higher-energy channels formed by AC and AD regions exhibit elliptical dispersion in the ground-state exciton frequency.

Such a control of the hyperbolicity range may help future experiments towards the actual observation of in-plane hyperbolic exciton-polariton propagation in few-layer BP in future experiments, as well as its technological application in future optoelectronic devices. Moreover, the hyperbolicity discussed here for exciton polaritons in BP is also expected to occur in other in-plane anisotropic semiconductors where excitonic peaks are equally narrow and strong, such as the recently synthesized trichalcogenides TiS_3 and ZrS_3 [51–53]. A proper analysis of the conditions for the emergence of hyperbolic exciton polaritons in these materials also comprises an exciting perspective for future research in polaritonics.

ACKNOWLEDGMENTS

Discussions with Tony Low, Francois M. Peeters, and Engin Torun are gratefully acknowledged. This work was supported by the Research Foundation - Flanders (FWO) and the Brazilian National Council for Scientific and Technological Development (CNPq), through the PRONEX/FUNCAP, Universal (Grant No. 423423/2021-5), and PQ (Grants No. 312705/2022-0 and No. 316081/2023-0) programs, and the CNPq Grant 142541/2020-6. M.V.M. gratefully acknowledges support from the Brazilian National Council for the Improvement of Higher Education (CAPES), and the CNPq-INCT National Institute of Science and Technology on Materials Informatics, Grant No. 371610/2023-0. The computer resources used in this work are provided by the University of Antwerp (CalcUA), a division of the Flemish Supercomputer Center (VSC), which is funded by the Hercules foundation, and the National Laboratory for Scientific Computing (LNCC/MCTI, Brazil).

[1] A. Castellanos-Gomez, Black phosphorus: Narrow gap, wide applications, J. Phys. Chem. Lett. **6**, 4280 (2015).

[2] J. Qiao, X. Kong, Z.-X. Hu, F. Yang, and W. Ji, High-mobility transport anisotropy and linear dichroism in few-layer black phosphorus, Nat. Commun. **5**, 4475 (2014).

[3] V. Tran, R. Soklaski, Y. Liang, and L. Yang, Layer-controlled band gap and anisotropic excitons in few-layer black phosphorus, Phys. Rev. B **89**, 235319 (2014).

[4] X. Wang, A. M. Jones, K. L. Seyler, V. Tran, Y. Jia, H. Zhao, H. Wang, L. Yang, X. Xu, and F. Xia, Highly anisotropic and robust excitons in monolayer black phosphorus, Nat. Nanotechnol. **10**, 517 (2015).

[5] A. Chernikov, T. C. Berkelbach, H. M. Hill, A. Rigosi, Y. Li, Ö. B. Aslan, D. R. Reichman, M. S. Hybertsen, and T. F. Heinz, Excitons in atomically thin transition-metal dichalcogenides, in *2014 Conference on Lasers and Electro-Optics (CLEO)-Laser Science to Photonic Applications* (IEEE, New York, 2014), pp. 1–2.

[6] O. A. Ajayi, J. V. Ardelean, G. D. Shepard, J. Wang, A. Antony, T. Taniguchi, K. Watanabe, T. F. Heinz, S. Strauf, X. Zhu *et al.*, Approaching the intrinsic photoluminescence linewidth in transition metal dichalcogenide monolayers, 2D Mater. **4**, 031011 (2017).

[7] H. Wang, A. Kumar, S. Dai, X. Lin, Z. Jacob, S.-H. Oh, V. Menon, E. Narimanov, Y. Kim, J.-P. Wang, P. Avouris, L. Moreno, J. Caldwell, and T. Low, Planar hyperbolic polaritons in 2D van der Waals materials, Nat. Commun. **15**, 69 (2024).

[8] T. Low, A. Chaves, J. D. Caldwell, A. Kumar, N. X. Fang, P. Avouris, T. F. Heinz, F. Guinea, L. Martin-Moreno, and F. Koppens, Polaritons in layered two-dimensional materials, Nat. Mater. **16**, 182 (2017).

[9] X. Liu, T. Galfsky, Z. Sun, F. Xia, E.-c. Lin, Y.-H. Lee, S. Kéna-Cohen, and V. M. Menon, Strong light–matter coupling in two-dimensional atomic crystals, Nat. Photonics **9**, 30 (2015).

[10] G. Lu, Z. Pan, C. R. Gubbin, R. A. Kowalski, S. De Liberato, D. Li, and J. D. Caldwell, Launching and manipulation of higher-order in-plane hyperbolic phonon polaritons in low-dimensional heterostructures, Adv. Mater. **35**, 2300301 (2023).

[11] J. Huang, L. Tao, N. Dong, H. Wang, S. Zhou, J. Wang, X. He, and K. Wu, In-plane hyperbolic phonon-polaritons in van der Waals nanocrystals, Adv. Opt. Mater. **11**, 2202048 (2023).

[12] W. Huang, T. G. Folland, F. Sun, Z. Zheng, N. Xu, Q. Xing, J. Jiang, H. Chen, J. D. Caldwell, H. Yan *et al.*, In-plane hyperbolic polariton tuners in terahertz and long-wave infrared regimes, Nat. Commun. **14**, 2716 (2023).

[13] Y. Xie, C. Wang, F. Fei, Y. Li, Q. Xing, S. Huang, Y. Lei, J. Zhang, L. Mu, Y. Dai *et al.*, Tunable optical topological transitions of plasmon polaritons in WTe_2 van der waals films, Light Sci. Appl. **12**, 193 (2023).

[14] M. Dehdast, Z. Valiollahi, M. Neek-Amal, B. Van Duppen, F. Peeters, and M. Pourfath, Tunable natural terahertz and mid-infrared hyperbolic plasmons in carbon phosphide, Carbon **178**, 625 (2021).

[15] G. Jia, J. Luo, H. Wang, Q. Ma, Q. Liu, H. Dai, and R. Asgari, Two-dimensional natural hyperbolic materials: From polaritons modulation to applications, Nanoscale **14**, 17096 (2022).

[16] E. van Veen, A. Nemilentsau, A. Kumar, R. Roldán, M. I. Katsnelson, T. Low, and S. Yuan, Tuning two-dimensional hyperbolic plasmons in black phosphorus, Phys. Rev. Appl. **12**, 014011 (2019).

[17] D. Basov, M. Fogler, and F. García de Abajo, Polaritons in van der Waals materials, Science **354**, aag1992 (2016).

[18] W. Ma, B. Shabbir, Q. Ou, Y. Dong, H. Chen, P. Li, X. Zhang, Y. Lu, and Q. Bao, Anisotropic polaritons in van der Waals materials, InfoMat **2**, 777 (2020).

[19] A. Sternbach, S. Chae, S. Latini, A. Rikhter, Y. Shao, B. Li, D. Rhodes, B. Kim, P. J. Schuck, X. Xu *et al.*, Programmable hyperbolic polaritons in van der Waals semiconductors, Science **371**, 617 (2021).

[20] P. Guo, W. Huang, C. C. Stoumpos, L. Mao, J. Gong, L. Zeng, B. T. Diroll, Y. Xia, X. Ma, D. J. Gosztola *et al.*, Hyperbolic dispersion arising from anisotropic excitons in two-dimensional perovskites, Phys. Rev. Lett. **121**, 127401 (2018).

[21] F. Wang, C. Wang, A. Chaves, C. Song, G. Zhang, S. Huang, Y. Lei, Q. Xing, L. Mu, Y. Xie *et al.*, Prediction of hyperbolic exciton-polaritons in monolayer black phosphorus, Nat. Commun. **12**, 5628 (2021).

[22] A. Marini, C. Hogan, M. Grüning, and D. Varsano, yambo: An *ab initio* tool for excited state calculations, Comput. Phys. Commun. **180**, 1392 (2009).

[23] L. Hedin and S. Lundqvist, *Effects of Electron-Electron and Electron-Phonon Interactions on the One-Electron States of Solids* (Academic, New York, 1970), pp. 1–181.

[24] G. Onida, L. Reining, and A. Rubio, Electronic excitations: density-functional versus many-body Green's-function approaches, Rev. Mod. Phys. **74**, 601 (2002).

[25] V. Hernandez, J. E. Roman, and V. Vidal, Slepc: A scalable and flexible toolkit for the solution of eigenvalue problems, ACM Trans. Math. Softw. **31**, 351 (2005).

[26] S. Ismail-Beigi, Truncation of periodic image interactions for confined systems, Phys. Rev. B **73**, 233103 (2006).

[27] A. N. Rudenko and M. I. Katsnelson, Quasiparticle band structure and tight-binding model for single-and bilayer black phosphorus, Phys. Rev. B **89**, 201408(R) (2014).

[28] V. Tran, R. Fei, and L. Yang, Quasiparticle energies, excitons, and optical spectra of few-layer black phosphorus, 2D Mater. **2**, 044014 (2015).

[29] P.-F. Loos and X. Blase, Dynamical correction to the Bethe–Salpeter equation beyond the plasmon-pole approximation, J. Chem. Phys. **153**, 114120 (2020).

[30] F. Caruso and F. Giustino, The GW plus cumulant method and plasmonic polarons: Application to the homogeneous electron gas, Eur. Phys. J. B **89**, 238 (2016).

[31] A. Bostwick, F. Speck, T. Seyller, K. Horn, M. Polini, R. Asgari, A. H. MacDonald, and E. Rotenberg, Observation of plasmarons in quasi-freestanding doped graphene, Science **328**, 999 (2010).

[32] P. Giannozzi, O. Baseggio, P. Bonfà, D. Brunato, R. Car, I. Carnimeo, C. Cavazzoni, S. de Gironcoli, P. Delugas, F. Ferrari Ruffino, A. Ferretti, N. Marzari, I. Timrov, A. Urru, and S. Baroni, Quantum espresso toward the exascale, J. Chem. Phys. **152**, 154105 (2020).

[33] J. P. Perdew, K. Burke, and M. Ernzerhof, Generalized gradient approximation made simple, Phys. Rev. Lett. **77**, 3865 (1996).

[34] D. R. Hamann, Optimized norm-conserving Vanderbilt pseudopotentials, Phys. Rev. B **88**, 085117 (2013).

[35] M. van Setten, M. Giantomassi, E. Bousquet, M. Verstraete, D. Hamann, X. Gonze, and G.-M. Rignanese, The PSEUDODOJO: Training and grading a 85 element optimized norm-conserving pseudopotential table, Comput. Phys. Commun. **226**, 39 (2018).

[36] S. Grimme, Semiempirical GGA-type density functional constructed with a long-range dispersion correction, J. Comput. Chem. **27**, 1787 (2006).

[37] V. Barone, M. Casarin, D. Forrer, M. Pavone, M. Sambi, and A. Vittadini, Role and effective treatment of dispersive forces in materials: Polyethylene and graphite crystals as test cases, J. Comput. Chem. **30**, 934 (2009).

[38] A. Molina-Sánchez, G. Catarina, D. Sangalli, and J. Fernández-Rossier, Magneto-optical response of chromium trihalide monolayers: Chemical trends, J. Mater. Chem. C **8**, 8856 (2020).

[39] P. Cudazzo, I. V. Tokatly, and A. Rubio, Dielectric screening in two-dimensional insulators: Implications for excitonic and impurity states in graphane, Phys. Rev. B **84**, 085406 (2011).

[40] D. Sangalli, A. Ferretti, H. Miranda, C. Attaccalite, I. Marri, E. Cannuccia, P. Melo, M. Marsili, F. Paleari, A. Marrazzo *et al.*, Many-body perturbation theory calculations using the yambo code, J. Phys.: Condens. Matter **31**, 325902 (2019).

[41] G. Kresse, M. Marsman, and J. Furthmüller, *VASP the GUIDE* (Universität Wien, Wien, Austria, Vienna, 2012).

[42] E. E. Salpeter and H. A. Bethe, A relativistic equation for bound-state problems, Phys. Rev. **84**, 1232 (1951).

[43] M. A. Mojarro, R. Carrillo-Bastos, and J. A. Maytorena, Hyperbolic plasmons in massive tilted two-dimensional Dirac materials, Phys. Rev. B **105**, L201408 (2022).

[44] G. Zhang, S. Huang, A. Chaves, C. Song, V. O. Özçelik, T. Low, and H. Yan, Infrared fingerprints of few-layer black phosphorus, Nat. Commun. **8**, 14071 (2017).

[45] G. Zhang, A. Chaves, S. Huang, F. Wang, Q. Xing, T. Low, and H. Yan, Determination of layer-dependent exciton binding energies in few-layer black phosphorus, Sci. Adv. **4**, eaap9977 (2018).

[46] G. Zhang, S. Huang, F. Wang, Q. Xing, C. Song, C. Wang, Y. Lei, M. Huang, and H. Yan, The optical conductivity of few-layer black phosphorus by infrared spectroscopy, Nat. Commun. **11**, 1847 (2020).

[47] G. Zhang, S. Huang, A. Chaves, and H. Yan, Black phosphorus as tunable van der Waals quantum wells with high optical quality, ACS Nano **17**, 6073 (2023).

[48] J. Quereda, P. San-Jose, V. Parente, L. Vaquero-Garzon, A. J. Molina-Mendoza, N. Agraït, G. Rubio-Bollinger, F. Guinea, R. Roldán, and A. Castellanos-Gomez, Strong modulation of optical properties in black phosphorus through strain-engineered rippling, Nano Lett. **16**, 2931 (2016).

[49] A. Manjanatha, A. Samanta, T. Pandey, and A. K. Singh, Semiconductor to metal transition in bilayer phosphorene under normal compressive strain, Nanotechnology **26**, 075701 (2015).

[50] I. Soltero, J. Guerrero-Sánchez, F. Mireles, and D. A. Ruiz-Tijerina, Moiré band structures of twisted phosphorene bilayers, Phys. Rev. B **105**, 235421 (2022).

[51] E. Torun, H. Sahin, A. Chaves, L. Wirtz, and F. M. Peeters, *Ab initio* and semiempirical modeling of excitons and trions in monolayer TiS_3, Phys. Rev. B **98**, 075419 (2018).

[52] A. Pant, E. Torun, B. Chen, S. Bhat, X. Fan, K. Wu, D. P. Wright, F. M. Peeters, E. Soignard, H. Sahin *et al.*, Strong dichroic emission in the pseudo one dimensional material ZrS_3, Nanoscale **8**, 16259 (2016).

[53] N. V. Morozova, I. V. Korobeinikov, K. V. Kurochka, A. N. Titov, and S. V. Ovsyannikov, Thermoelectric properties of compressed titanium and zirconium trichalcogenides, J. Phys. Chem. C **122**, 14362 (2018).